Towards Personalized Interventional SPECT-CT Imaging

José Gardiazabal[1,2], Marco Esposito[1], Philipp Matthies[1], Aslı Okur[1,2], Jakob Vogel[1], Silvan Kraft[1,3], Benjamin Frisch[1], Tobias Lasser[1], and Nassir Navab[1,4]

[1] Computer Aided Medical Procedures (CAMP)
[2] Department of Nuclear Medicine, Klinikum Rechts der Isar
[3] Department of Radiology, Klinikum Rechts der Isar
Technische Universität München, Germany
[4] Computer Aided Medical Procedures (CAMP),
Johns Hopkins University, USA

Abstract. The development of modern robotics and compact imaging detectors allows the transfer of diagnostic imaging modalities to the operating room, supporting surgeons to perform faster and safer procedures. An intervention that currently suffers from a lack of interventional imaging is radioembolization, a treatment for hepatic carcinoma. Currently, this procedure requires moving the patient from an angiography suite for preliminary catheterization and injection to a whole-body SPECT/CT for leakage detection, necessitating a second catheterization back in the angiography suite for the actual radioembolization. We propose an imaging setup that simplifies this procedure using a robotic approach to directly acquire an interventional SPECT/CT in the angiography suite. Using C-arm CT and a co-calibrated gamma camera mounted on a robotic arm, a personalized trajectory of the gamma camera is generated from the C-arm CT, enabling an interventional SPECT reconstruction that is inherently co-registered to the C-arm CT. In this work we demonstrate the feasibility of this personalized interventional SPECT/CT imaging approach in a liver phantom study.

1 Introduction

Traditional medical imaging systems often employ a single contrast mechanism like ultrasound reflection, X-ray transmission (CT), magnetic resonance (MRI), single photon (SPECT) or positron emission (PET). These single-modality devices are able to provide medically useful pictures of almost any organ, but can have unfavorable side effects such as limited resolution, sub-optimal contrast or lack of anatomical references. In terms of interventional imaging, single-modality devices such as robotic C-arm CT [1] or freehand SPECT [2] are used very successfully in clinical practice on a regular basis.

In the past 15 years, dual-modality systems that combine anatomic (like CT or MRI) with functional imaging (like SPECT or PET) have become increasingly common [3]. Such devices provide naturally co-registered datasets and enable

P. Golland et al. (Eds.): MICCAI 2014, Part I, LNCS 8673, pp. 504–511, 2014.

optimal fusion of information. The typical layout as whole-body gantry-based scanners, however, limits their use in organ-specific imaging and prevents most interventional applications, despite a number of possible scenarios where interventional dual-modality imaging would be highly desirable.

One particular example of such an interventional application is brachytherapy of unresectable liver tumors, like hepatocellular carcinoma (HCC). Brachytherapy in the form of radioembolization (Selective Internal RadioTherapy – SIRT) is an alternative to classical chemoembolization or chemotherapy [4]. In this case, microspheres loaded with ^{90}Y are injected into the hepatic arteries using a catheter for selective internal irradiation of the tumor cells. ^{90}Y mainly undergoes β^- decay, emitting electrons that are absorbed within at most 11 mm of tissue, making it possible to inject very high doses within a single treatment. It is, however, crucial to ensure that the radioactive compound remains confined to the injection site in order to irradiate only the surrounding cancer tissue. Any leakage to other parts of the liver or other organs, for example through a shunt to the lung, must be prevented.

The current practice is to inject ^{99m}Tc-MAA through a catheter first, which has demonstrated good prognostic value for the ^{90}Y distribution [5]. The patient is then transferred from the radiology department, where the catheterization and injection take place, to the nuclear medicine department for a whole-body SPECT scan, usually combined with CT, to monitor the ^{99m}Tc distribution. This process takes four to six hours on average and requires, if the result is positive, a second intervention in the radiology department with another catheterization for the actual radioembolization with ^{90}Y itself.

As shown by this example, the use of a diagnostic device incurs organizational complexity and prolongs the duration of the intervention. For this reason, we propose a novel approach to interventional SPECT/CT imaging consisting of a C-arm CT scanner and a robot-controlled gamma camera, where the latter's trajectory is optimized based on the patient's anatomy as extracted from the C-arm CT data. This approach enables clinicians to perform interventions like radioembolization on a single site and during a single procedure, substantially reducing patient stress and time commitment of the medical personnel. On top of this, the core imaging process also benefits from this fusion, as the required data can be collected very efficiently in a patient-specific manner, leading to equivalent medical information significantly faster and with similar accuracy as currently available in the state-of-the-art whole-body scenario.

This paper shows the feasibility of the combined interventional C-arm CT/robotic SPECT approach in an experimental liver phantom setting close to the clinical application.

2 Materials and Methods

2.1 Overview

As shown in Fig. 1, we extend an angiography suite by placing a robot-mounted multi-channel gamma camera next to the C-arm. Using appropriate calibration

techniques as detailed in section 2.2, we can acquire all relevant data, X-ray transmission and gamma radiation, with respect to a single, common coordinate frame.

With this setup in place and calibrated, we first acquire a CT image of the volume of interest. Based on it, we extract the convex hull of the patient's (or phantom's) surface and compute an optimal trajectory for acquiring the SPECT images from minimal, but safe distances. Finally, we record the emission data by moving the gamma camera along the trajectory using the robotic arm and reconstruct the tracer distribution using likelihood-based tomographic reconstruction, as described in section 2.4.

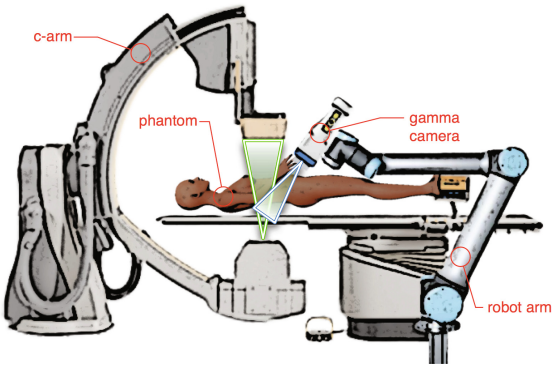

Fig. 1. Combined C-arm CT and robotic SPECT setup in the operating room

2.2 Coordinate Systems Calibration

In order to use the C-arm system without modifications, we assume its coordinate system as the reference. Consequently, we need to obtain the rigid transformation between the robot's base and the C-arm coordinate system.

For this purpose, we mount a custom-designed calibration target, shown in Fig. 2a, to the robot's wrist, as shown in Fig. 2b. The target contains highly visible spheres in a well-defined pattern, that can be segmented easily in the CT volume. Using point-based registration as suggested by Umeyama [6], we obtain the transformation between the CT image and the calibration target, which can be propagated to the robot's base thanks to the precisely known dimensions and joint angles via forward kinematics.

2.3 Trajectory Planning

The first step of the core acquisition protocol consists of recording the X-ray component of the joint signal by rotating the C-arm over 180° around the region of interest and reconstructing it into a 3D volume.

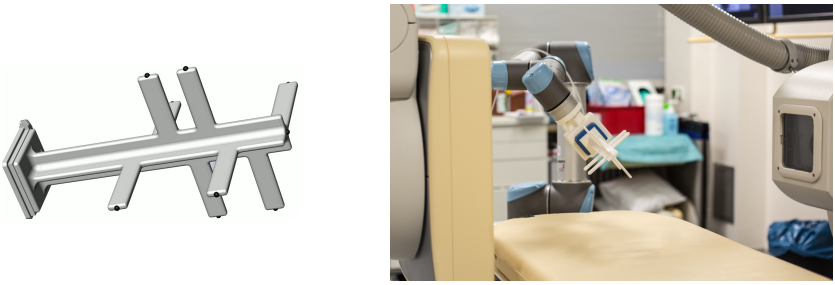

(a) Calibration tool (b) Calibration setup

Fig. 2. a) CAD drawing of the calibration tool and b) setup used to map the C-arm coordinate system to the robot coordinate system. The spheres attached to the fins appear prominently in the CT volume and can be easily segmented.

In a second step, we compute a model of the patient's (or phantom's) surface from the CT image. As X-ray transmission through the surrounding air is significantly higher than through tissue, it is possible to distinguish both regions by applying a threshold. The convex hull is then a suitable mesh-model for the surface.

Finally, the trajectories are generated as three parallel scan-lines normal to the convex hull of the patient (up to a certain security distance, 1 cm in this case), as shown in Fig. 3. Note that, unlike a fixed gantry in diagnostic SPECT, the camera poses are much closer for a personalized trajectory with better detection statistics.

2.4 Image Reconstruction

Having collected the emission values by moving the camera along the acquisition trajectory, the final task is the reconstruction of the SPECT image. Considering the Poisson-distribution of the measured values m_j, we compute the maximum-likelihood estimate

$$\arg\max_{\mathbf{x}} \left(\sum_{j=1}^{m} m_j \log(\overline{m}_j(\mathbf{x})) - \overline{m}_j \right)$$

where $\overline{m}_j(\mathbf{x})$ denotes the expected measurement given a reconstruction $\mathbf{x}$. The solution to this optimization problem can be obtained in several ways, and we apply Maximum Likelihood Expectation Maximization (MLEM) as suggested by Shepp and Vardi [7]. An important aspect of this process is an accurate model of the camera's measurement probabilities, usually referred to as the forward model. We employ the procedure proposed in [8]that uses high-resolution lookup tables collected during long-term calibration measurements.

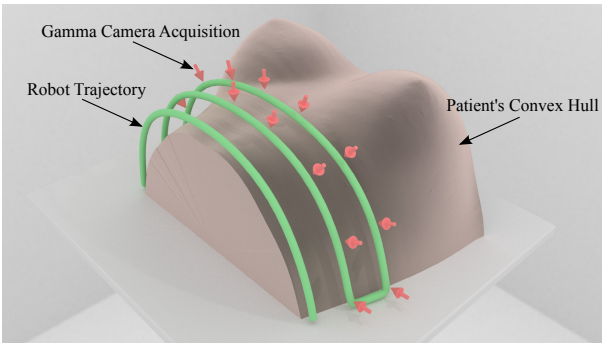

Fig. 3. Schematic representation of a personalized trajectory for the robot-guided gamma camera along the convex hull of the patient/phantom as extracted from CT. The green line represents the planned robot trajectory, that follows the convex hull plus the safety margin (1 cm), the red arrows indicate positions where the gamma camera acquires images.

The X-ray CT reconstruction is directly obtained from the software solution of the C-arm manufacturer, and is based on Feldkamp's variant of Filtered Back-Projection [9]. As the SPECT measurements have been collected relative to the C-arm's coordinate frame, the two volumetric images are inherently aligned.

3 Experiments

3.1 Setup

The imaging setup consists of a C-arm CT and a mini gamma camera mounted on a robotic arm, as illustrated in Fig. 1. The C-arm CT is a Philips Allura Xper FD20 set up in an angiography room. The mini gamma camera (Crystal Imager, Crystal Photonics, Germany) uses a $4 \times 4\,\mathrm{cm}^2$ CdZnTe crystal detector segmented into 16×16 pixels. The camera is mounted on a robotic arm (UR5, Universal Robots, Denmark) placed next to the C-arm, see Fig. 4b.

3.2 Experimental Procedure

Verification experiment. In a first experiment, we verify the quality of our calibration procedure. We attach a single ^{57}Co point source to a torso phantom and obtain a CT image. Based on the location of the point source segmented from the CT image, we instruct the robot with the gamma camera to acquire a single image centered on the point source. The expected result is a gamma camera image with the point source showing as a hotspot in the center.

Reconstruction experiment. In a second experiment, we place a human torso phantom with a liver model made out of candle gel (Ceraflex N 530 transparent,

Wachs- und Ceresinfabriken, Germany) on the exam table. Liver arteries are imitated by plastic tubes (4 mm diameter), filled with 4 MBq of ^{99m}Tc.

We obtain a CT image of the torso and compute the trajectory for the SPECT acquisition according to the procedure described in section 2.3. The emission data recorded by the robot-positioned gamma camera is reconstructed as an image inherently co-registered with the CT image. We expect to see the liver arteries in the reconstructed SPECT image embedded in the anatomical information from the CT.

4 Results

Verification experiment. Fig. 4a shows a planar scintigraphy of the ^{57}Co source, acquired with the gamma camera instructed to point its center at the source (see Fig. 4b), based on the source position as detected from the C-arm CT as well as the coordinate system calibration. The relocalization error, i.e. the offset from the hotspot's center of mass to the center of the image, is 1.6 camera pixels (corresponding to 3.9 mm).

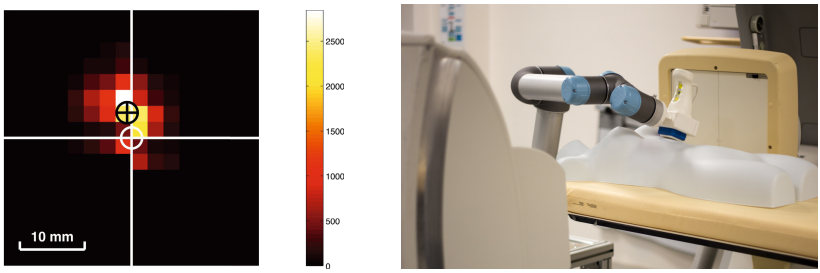

(a) Gamma camera image of point source

(b) Photo of gamma camera acquiring image shown in (a)

Fig. 4. Result of calibration verification experiment

Reconstruction experiment. Fig. 5a shows a 3D rendering of the robotic SPECT image of our phantom. The branching blood-vessels simulated by three activity-filled tubes are clearly distinguishable. The co-registered robotic SPECT/C-arm CT slice image in Fig. 5b shows that the offset between the tubes in the SPECT and the CT image is minimal.

5 Discussion

Calibration of the C-arm and gamma camera coordinate systems is a vital part of the imaging protocol. Our first experiment validates our approach, as the relocalization error is within the acceptable error limit for interventions. In addition to this, we performed a comparable experiment under guidance of an optical tracking system and only achieved considerably higher errors.

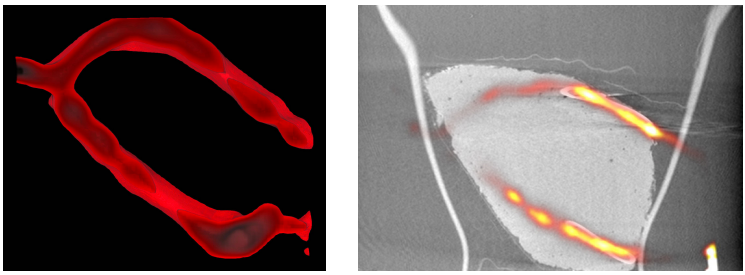

(a) Robotic SPECT (b) Slice of fused SPECT/CT

Fig. 5. (a) 3D rendering of the SPECT image of the liver phantom with radioactive blood vessels and (b) slice of fused robotic SPECT/C-arm CT

The second experiment confirms the possibility of acquiring bi-modal interventional robotic SPECT and C-arm CT images in a clinical environment, with a realistic liver phantom. We were able to extract a patient-specific acquisition trajectory based on the convex hull of the torso and record a SPECT image that is naturally aligned to the C-arm CT image.

Our setup is limited by the C-arm that does not allow any customization of the acquisition protocol. A C-arm CT mounted on a robotic arm [1] would overcome this limitation, provided that the respective control interface is accessible. It would further allow to define personalized C-arm CT acquisition trajectories as suggested by Stayman et al. [10]. Also, the spectrum-based trajectory optimization for SPECT as proposed by Vogel et al. [11] could be considered. Both would lead to fully personalized interventional SPECT/CT acquisition.

6 Conclusion

This paper presents the first prototype for an interventional SPECT/CT scanner. We believe the quality is good enough to be used in an intra-operative scenario. In recent times, the community has shown considerable interest in such a device, and simulation studies have been published, for instance by Bowsher et al. [12] where a much heavier robot is used that cannot easily be removed or transferred. Our design is very light, thus meeting the accessibility and flexibility requirements of clinical practice.

The advantages of interventional SPECT/CT are obvious: the duration and complexity of interventions are substantially reduced, the progress can be monitored in an easy and flexible way (for instance, by acquiring a bremsstrahlung SPECT image [13]). The latter can also be used to quickly detect aberrations such as leaks, thus enabling effective quality control.

The suggested method is ready for further investigation in the operating room, opening the path for alternative applications, for example in the head and neck region.

Acknowledgements. This work was partially funded by the DFG cluster of excellence MAP, the TUM Institute for Advanced Study (funded by the German Excellence Initiative), and the Bayerische Forschungsstiftung (project RoBildOR). We want to thank Alexandru Duliu for his assistance with Blender.

References

1. Ganguly, A., Fieselmann, A., Marks, M., Rosenberg, J., Boese, J., Deuerling-Zheng, Y., Straka, M., Zaharchuck, G., Bammer, R., Fahrig, R.: Cerebral CT Perfusion Using an Interventional C-Arm Imaging System: Cerebral Blood Flow Measurements. Am. J. Neuroradiol. 32, 1525–1531 (2011)
2. Wendler, T., Herrmann, K., Schnelzer, A., Lasser, T., Traub, J., Kutter, O., Ehlerding, A., Scheidhauer, K., Schuster, T., Kiechle, M., Schwaiger, M., Navab, N., Ziegler, S.I., Buck, A.K.: First demonstration of 3-D lymphatic mapping in breast cancer using freehand SPECT. Eur. J. Nucl. Med. 37(8), 1452–1461 (2010)
3. Cherry, S.R., Sorenson, J.A., Phelps, M.E.: Physics in Nuclear Medicine. Elsevier Health Sciences (April 2012)
4. Sangro, B., Iñarrairaegui, M., Bilbao, J.I.: Radioembolization for hepatocellular carcinoma. Journal of Hepatology 56(2), 464–473 (2012)
5. Lam, M.G.E.H., Goris, M.L., Iagaru, A.H., Mittra, E.S., Louie, J.D., Sze, D.Y.: Prognostic Utility of 90Y Radioembolization Dosimetry Based on Fusion 99mTc-Macroaggregated Albumin-99mTc-Sulfur Colloid SPECT. Journal of Nuclear Medicine 54(12), 2055–2061 (2013)
6. Umeyama, S.: Least-squares estimation of transformation parameters between two point patterns. IEEE Transactions on Pattern Analysis and Machine Intelligence 13(4), 376–380 (1991)
7. Shepp, L.A., Vardi, Y.: Maximum Likelihood Reconstruction for Emission Tomography. Transactions on Medical Imaging MI-1(2), 113–122 (1982)
8. Matthies, P., Gardiazabal, J., Okur, A., Vogel, J., Lasser, T., Navab, N.: Mini Gamma Cameras for Intra-operative Nuclear Tomographic Reconstruction Medical Image Analysis (2014)
9. Feldkamp, L.A., Davis, L.C., Kress, J.W.: Practical cone-beam algorithm. Journal of the Optical Society of America A 1(6), 612–619 (1984)
10. Stayman, J., Siewerdsen, J.: Task-based trajectories in iteratively reconstructed interventional cone-beam CT, Lake Tahoe, CA, pp. 257–260 (2013)
11. Vogel, J., Lasser, T., Gardiazabal, J., Navab, N.: Trajectory optimization for intra-operative nuclear tomographic imaging. Medical Image Analysis 17(7), 723–731 (2013)
12. Bowsher, J., Yan, S., Roper, J., Giles, W., Yin, F.F.: Onboard functional and molecular imaging: a design investigation for robotic multipinhole SPECT. Medical Physics 41(1), 010701 (2014), PMID: 24387490 PMCID: PMC3888458
13. Ahmadzadehfar, H., Muckle, M., Sabet, A., Wilhelm, K., Kuhl, C., Biermann, K., Haslerud, T., Biersack, H.J., Ezziddin, S.: The significance of bremsstrahlung SPECT/CT after yttrium-90 radioembolization treatment in the prediction of extrahepatic side effects. European Journal of Nuclear Medicine and Molecular Imaging (October 2011), PMID: 21975832